Atlas-Based Automated Positioning of Outer Volume Suppression Slices in Short-TE 3D MR Spectroscopic Imaging of the Human Brain

Journal:	*Magnetic Resonance in Medicine*
Manuscript ID:	Draft
Wiley - Manuscript type:	Full paper
Date Submitted by the Author:	n/a
Complete List of Authors:	Yung, Kaung-Ti; The University of New Mexico, Dept. of Neurology Zheng, Weili; The University of New Mexico, Dept. of Neurology Zhao, Chenguang; The University of New Mexico, Dept. of Neurology van der Kouwe, André; Athinoula A. Martinos Center, Radiology Martinez-Ramon, Manel; Universidad Carlos III de Madrid, Teoria de la Senal y Comunicaciones Posse, Stefan; The University of New Mexico, Dept. of Neurology
Research Type:	Technique Development < Technical Research, Spectroscopy/Spectroscopic Imaging < Technique Development < Technical Research
Research Focus:	Brain < Neurological, Normal < Anatomy < Brain < Neurological

Atlas-Based Automated Positioning of Outer Volume Suppression Slices in Short-TE 3D MR Spectroscopic Imaging of the Human Brain

[1]Kaung-Ti Yung, [1]Weili Zheng, [1]Chenguang Zhao, [2]Manel Martínez-Ramón, [3]Andre van der Kouwe, and [1,4,5]Stefan Posse

1. Dept. of Neurology, University of New Mexico School of Medicine, Albuquerque, NM, USA.
2. Dept. of Signal Theory and Communications, Universidad Carlos III de Madrid, Leganés, Madrid, Spain.
3. Athinoula A. Martinos Center for Biomedical Imaging, Massachusetts General Hospital, Charlestown, Massachusetts, USA
4. Dept. of Electrical and Computer Engineering University of New Mexico, Albuquerque, NM, USA.
5. Dept. of Physics and Astronomy, University of New Mexico, Albuquerque, NM, USA

Corresponding author: Stefan Posse, Dept. of Neurology, The University of New Mexico School of Medicine, 1 University of New Mexico, MSC 105620, Albuquerque, NM, USA. E-mail address: sposse@unm.edu

Running Head: Atlas-Based Automated Positioning of Outer Volume Suppression Slices in MR Spectroscopic Imaging

Number of words: 7449

Keywords: MR spectroscopic imaging, lipid suppression, outer volume suppression, affine transformation, brain atlas

Abstract

Spatial suppression of peripheral lipid-containing regions in volumetric MR spectroscopic imaging (MRSI) of the human brain requires placing large numbers of outer volume suppression (OVS) slices, which is time consuming, prone to operator error and may introduce subject-dependent variability in volume coverage. We developed a novel, computationally efficient atlas-based approach for automated positioning of up to 16 OVS slices and the MRSI slab. Standardized positions in MNI atlas space were established offline using a recently developed iterative optimization procedure. During the scanning session, positions in subject space were computed using affine transformation of standardized positions in MNI space. This atlas-based approach was characterized offline using MPRAGE data collected in 11 subjects. The method was further validated in 14 subjects on a clinical 3T scanner using 3D short TE (15-20ms) Proton-Echo-Planar-Spectroscopic-Imaging (PEPSI) in upper cerebrum. Comparison of manual and automatic placement using 8 OVS slices demonstrated consistent MRSI volume selection and comparable spectral quality with similar degree of lipid suppression and number of usable voxels. Automated positioning of 16 OVS slices enabled larger volume coverage, while maintaining similar spectral quality and lipid suppression. Atlas-based automatic prescription of short TE MRSI is expected to be advantageous for longitudinal and cross sectional studies.

Number of words: 200

Introduction

Suppression of overwhelming lipid and water signals from peripheral regions around the brain is necessary in proton MR spectroscopic imaging (MRSI) to prevent spectral contamination inside the volume of interest (VOI) due to the point spread function. Outer volume suppression (OVS) using spatial pre-saturation [1-16] is widely employed for MRSI studies on clinical scanners and the state of the art in method development has focused on improving the suppression efficiency by optimizing RF pulse design, gradient switching schemes and timing of OVS modules. Recently, Henning et al. [13, 14] developed powerful T1- and B1-insensitive outer volume suppression methods with highly selective broadband RF pulses to minimize chemical shift displacement artifacts at high field. Our group has shown the feasibility of ultra-short echo time (TE) high-speed MRSI in human brain using slice-selective Proton-Echo-Planar-Spectroscopic-Imaging (PEPSI) with eight OVS slices positioned along the periphery of the brain in [6, 7, 9, 12, 16].

However, positioning of suppression slices in these studies was performed manually, which introduced operator-dependent and possible inter-subject and intra-subject variability of the VOI. Although, Duyn et al. [4] introduced semi-automatic placement of 8 OVS slices for multi-slice MRSI based on a user-defined octagon shaped VOI to facilitate clinical usage, for measurements at short TE in lateral cortical regions, this approach still demanded manual interventions to maximize volume coverage. Manual placement of OVS slices requires considerable skill and time to balance the needs of completely covering peripheral brain regions with a limited number of OVS saturation bands (to constrain T1-related losses in suppression) and minimizing the loss of lateral cortical brain regions while taking into consideration the OVS slice transition bandwidth and chemical shift artifacts. Optimal placement of OVS slices in triple-oblique orientation is hard to visualize on the scanner Graphical user Interface (GUI). Moreover, manually placing a large number of OVS slices for volumetric MRSI to obtain larger VOI coverage is even more challenging and may become unmanageable as the number of OVS slices increases. It is thus highly desirable to

automate the process of positioning optimal OVS slices. This is particularly important when tracking changes in lesion volume and related metabolic changes in clinical MRSI studies.

Automated methods for positioning multiple spatial saturation slices were designed by Ryner et al. [10] and Venugopal et al. [11] to delineate small volumes within a particular organ, such as around a breast lesion, prostate tumor or a brain tumor mass, but this methodology has not been applied to delineate an entire organ. Recently, we proposed an iterative optimization approach [16] to automatically place up to sixteen OVS slices in peripheral regions and demonstrated on a clinical 3T scanner the feasibility of automated short TE 3D MRSI in an individual's brain. The resultant metabolic maps and spectra of the automated placement method were comparable to those acquired from manually placed OVS slices by a skilled operator. Ozhinsky and Nelson presented an automatic prescription of an oblique PRESS box and 9 OVS slices to extend brain coverage ensuring effective lipid suppression at long TE [15]. These automatic methods [10, 11, 15, 16] are capable of accurate placement of OVS slices on a subject by subject basis, but they are subject to brain segmentation errors and local minima in optimization, which affects reliability and consistency, and they are time consuming. As a result, these methods do not guarantee consistent OVS coverage and region of interest (ROI) positioning, which limits their usefulness for investigating spectral changes in lateral cortical regions in longitudinal studies in individual subjects and in cross-sectional studies.

Inspired by the increasing use of statistical brain atlases in clinical settings for automatic positioning of MR imaging slices and the proven high efficiency, robustness and precision of the methodology [17, 18], we extended our recent work [16] with a new automatic method for OVS placement based on the use of a standardized atlas brain. In this approach, a template is created by placing the MRSI slab on the Montreal Neurological Institute (MNI) atlas brain [19] to specify the volume of interest (VOI) and by positioning up to 16 saturation bands on this brain atlas to suppress peripheral lipid around the VOI defined by this slab using the automatic placement method described in [16]. During an actual scanning session, both the MRSI slab and the OVS slices are converted by affine transformation to their

corresponding positions in the subject space using the FMRIB's Linear Image Registration Tool (FLIRT) implemented in the FMRIB's Software Library (FSL) [20]. The method was validated in the human brain in an offline analysis using previously acquired MPRAGE scans and up to 16 OVS slices. *In vivo* implementation in comparison to manual placement was tested on clinical 3T scanners in a multi-center study using 3D short TE (15-20 ms) Proton-Echo-Planar-Spectroscopic-Imaging (PEPSI) in upper cerebrum with automated spectral quantification based on LCModel fitting [21]. We compared the coverage of peripheral lipid containing regions and the suppression of cortical regions by OVS slices, the number of usable voxels with Cramer Rao lower bounds less than 20 %, and the quantification of metabolite maps for manual and automatic placement of the MRSI slab and up to 16 OVS slices.

Theory

The atlas-based prescription method in [17, 18], which is now available on clinical scanners of the major manufacturers, has shown its usefulness in clinical applications. With this method, the slices are first selected in a probabilistic atlas representing the population and then aligned to an online localizer based on the rigid body registration matrix between the low resolution localizer and the atlas. Unfortunately, the rigid body registration considers only rotation and translation, which is not applicable for OVS slice placement due to the need for very precise positioning in peripheral regions of the brain taking into account scaling and geometrical variability between the atlas brain and the subject brain. Therefore, it is necessary to use the affine transformation [20] or even nonlinear deformation [22].

Based on the framework of atlas-based slice prescription in [17,18], we propose a solution to automatically place the OVS slices online in 3D MRSI. In a first step the MRSI slab is placed in atlas space to define a VOI of specific clinical interest. The thickness and orientation of the slab is chosen based on the number of available OVS slices, the expected shimming conditions within the VOI and TE. Long TE MRSI scans are more tolerant to lipid contamination and magnetic field inhomogeneity, enabling the use of larger VOIs. Short TE

MRSI scans are less tolerant to magnetic field inhomogeneity, constraining the VOI size. The OVS slices are automatically placed using an optimization method [16] to completely cover lipid containing peripheral areas. During the actual MRSI scan session, high resolution structural scans of the subject are used to compute the affine transformation matrix between the atlas brain and the subject brain. Then the prescriptions of the MRSI slab and the OVS slices are mapped to subject space using the inverse of the affine transformation.

Placement of the MRSI slab and OVS slices in atlas space (offline)

The first step is to manually place the MRSI slab in the brain atlas to define the VOI. For short TE 3D MRSI in the upper cerebrum we positioned a thick slab in AC/PC orientation extending upwards from the middle of the ventricles to the top of the brain, which avoids frontal areas with large magnetic field inhomogeneity. The VOI is thus defined as the brain volume covered by the MRSI slab. This VOI may be changed according to the clinical interest, but shimming conditions *in vivo* need to be taken into consideration. In case of 16 OVS slices, two of the OVS slices were placed directly inferior and superior, in parallel to the MRSI slab in order to reduce edge artifact from imperfections of 3D RF excitation (Fig. 1). and the rest are placed automatically in two rings to form a convex hull as described in [16]. In case of 8 OVS slices a single ring is used. First, the lipid-containing peripheral regions in a brain atlas are identified using the brain/non-brain segmentation tools BET [22]. The performance of BET is satisfactory here due to the absence of intensity inhomogeneity and other artifacts in the template. Then the OVS slices are automatically placed using the iterative optimization method described in [16]. Note that this offline optimization procedure is performed only once for all subsequent in vivo scanning.

Registration of the subject head to the atlas head (online)

The registration problem here is to find the set of parameters describing the transformation matrix from the source image in subject space to the reference image in atlas space, which maximizes the “similarity” between these two images in atlas space. The transformation function could be a linear function [23, 24] or a combination of some nonlinear basis functions [25, 26]. Here we used FLIRT (FMRIB's Linear Image Registration Tool) [20], a

widely used fully automated robust and accurate tool, which uses an intensity based cost function for linear (affine) intra-modal structural brain image registration. To further improve the precision of registration, additional factors such as the interpolation method, the intensity inhomogeneity of subject images due to B1-inhomogeneity [20], orientations of images, and the symmetry of registration [27] were investigated (see below).

Transformation of the prescription of slices to subject space (online)

The affine transformation using FLIRT (in FSL package [20]) consists of translation, rotation, scaling and shear. The slice S in atlas space is defined by a normal vector *N*, which is represented by three orthogonal vectors (N_x, N_y, N_z), and the slice center (P_x, P_y, P_z) with respect to a generic 3D Cartesian coordinate system:

$$S = \begin{bmatrix} & & & P_x \\ N_x & N_y & N_z & P_y \\ & & & P_z \\ 0 & 0 & 0 & 1 \end{bmatrix} \quad (1)$$

The affine transformation generates a slice S' in subject space:

$$S' = M_r^{-1} S \quad (2)$$

, where the transformed center is represented by (P_x', P_y', P_z'). However, the transformed vectors (N_x', N_y', N_z') are no longer orthogonal if a shear transformation is involved. To account for this, three new orthogonal vectors (N_x'', N_y'', N_z'') are reconstructed as follows:

$$N_x'' = N_x'$$

$$N_z'' = N_x' \times N_y'$$

$$N_y'' = N_z' \times N_x' \quad (3)$$

where × is the vector product operator, used here to orthogonalize vectors N_y and N_z with respect to N_x.

The transformed slice S' is thus represented by

$$S' = \begin{bmatrix} N_x'' & N_y'' & N_z'' & P_x' \\ & & & P_y' \\ & & & P_z' \\ 0 & 0 & 0 & 1 \end{bmatrix} \quad (4)$$

In our implementation, the output OVS slice center and normal vectors were specified in accordance with the Siemens patient coordinate system LPS (Left-Posterior-Superior), which is used in the Siemens console GUI. The MNI template is in the Neurological (Right-Anterior-Superior = RAS) orientation and the FMRIB Software Library (FSL) uses the Radiological (Left-Anterior-Superior = LAS) coordinate system. To ensure internal consistency all intermediate images, transformations and prescription of slices conformed to RAS.

Materials and Methods

Implementation of the OVS placement pipeline

Note that the placement of the MRSI slab and the OVS slices in MNI space in Step 1 is carried out offline only once, while the subsequent steps are performed online for each subject brain during an *in vivo* MRSI experiment.

Step 1: The MNI template (MNI512_T1_1mm head [19]) was used in RAS orientation. The MRSI slab was manually placed on the MNI head and oriented in parallel with the AC-PC line (the anterior axis in the RAS coordinate system) extending in the superior direction (Fig.1). The slab thickness was chosen to be either 40 mm for the 8 OVS slice implementation or 52 mm for the 16 OVS slice implementation. This selection of slab thickness in vivo was chosen to maximize brain volume coverage while minimizing loss of cortical tissue and line broadening due to magnetic field inhomogeneity in inferior frontal cortex. For offline simulation the slab thickness for 16 OVS slice was increased to 80 mm to assess feasibility of covering a larger brain area extending in the inferior direction. The iterative optimization procedure for these OVS slices [16] yielded a slice thickness in MNI

space ranging from 19.2 mm to 22 mm. This thickness was manually extended to a uniform 25 mm, taking into consideration the finite transition width of the suppression slice profile and chemical shift displacement. The slice thickness of these two OVS slices was optimized manually to suppress signals from the nasal cavities (slice 1, inferior to the MRSI slab, thickness: 40 mm) and to fully cover superior lipid containing regions (slice 16, superior to the MRSI slab, thickness: 30 mm).

Step 2: High resolution T1-weighted structural scans acquired with the Siemens MPRAGE sequence were used to obtain the affine transformation matrix between the MNI brain and the subject brain. The MPRAGE scans in DICOM format were transferred to an external 64-bit Dell T7400 workstation and converted to a 3D volume in NIFTI1 format (.nii) using the FreeSurfer (version 3.0.4) (http://surfer.nmr.mgh.harvard.edu/) function mri_convert.

Step 3: It was necessary to adjust the image intensity profile to reduce adverse effects of intensity inhomogeneity on registration accuracy. The FreeSurfer module mri_nu_correct.mni was used to correct the image intensity inhomogeneity of the subject head 3D volume. It uses the Nonparametric Non-uniformity intensity Normalization method (N3) [28] that does not require a tissue model, is independent of pulse sequence and is insensitive to pathology.

Step 4: The inhomogeneity-corrected 3D volume was re-sliced to RAS orientation with a $1\times1\times1$ mm^3 voxel size using a Matlab routine reslice_nii, available for download from http://www.rotman-baycrest.on.ca/~jimmy/NIFTI/.

Step 5: The affine transformation matrix M_r was determined by registering the subject head to the MNI head using the FSL function FLIRT [20]. Here, M_r provided by FLIRT was defined in the native image coordinate system (centered at one of the image volume corners) instead of the RAS system.

Step 6: A Matlab script was developed in-house to map the prescription (center and normal vector) of the MRSI slab and the OVS slices in MNI space to subject space using the inverse of the above affine matrix M_r^{-1}

$$S' = M_s M_r^{-1} M_a^{-1} S \quad (5)$$

where M_s and M_a are the voxel to RAS transformation matrices between the subject brain and the MNI brain.

Step 6: For visualization purposes using fslview [20], the transformed prescriptions of the MRSI slab and OVS slices were reconstructed to form 3D slabs in the subject space that were overlaid on the high-resolution MPRAGE scan. The MRSI slab and OVS slice prescriptions were written to an ASCII file, which was transferred to the scanner console and read by a modified PEPSI pulse sequence (see below). The placement of the slices was shown superimposed on the subject's localizer scan by the scanner GUI.

Subjects and data acquisition

Fourteen healthy subjects participated after giving institutionally reviewed informed consent. Data were collected on Siemens 3T TIM Trio scanners (Siemens Medical Solutions, Inc.) equipped with Avanto gradient system and 12 channel array head coil. High-resolution T_1-weighted MPRAGE (Magnetization Prepared RApid Gradient Echo) scans were acquired with TR: 1810ms, TI: 900ms, TE: 2.52ms, flip angle: 8^o, bandwidth: 651Hz/Px, 160 or 192 sagittal slices with 256×256 in-plane resolution, and isotropic 1 mm voxel dimensions. High-resolution multi-slice T_2-weighted turbo spin-echo scans with the same slice orientation as the PEPSI scan were acquired for manual placement of the OVS slices. MRSI data acquisition was performed using the PEPSI pulse sequence descried in [12], using a spectral width of 1087 Hz and a digital spectral resolution of 1Hz. The GUI of the Siemens scanner allows manual placement of up to 8 OVS slices. For automated OVS placement the PEPSI sequence was modified to read the OVS slice offsets, rotation angles and thicknesses from a ASCII text file described above. The number of OVS modules was increased to 16, which required elongating the duration of the first two water suppression modules to maintain consistent timing of the water suppression modules. Gradient crusher orientations and amplitudes were carefully chosen to avoid secondary echoes. The GUI was modified to display a user selectable set of 8 of the 16 OVS slices overlaid on the T_2-weighted turbo spin-

echo scans to assess OVS slice placement. The MRSI slab origin and orientation were entered manually from the ASCII text file described above.

3D PEPSI data for comparing manual and automated placement of 8 OVS slices was collected from a 40 mm thick slab in AC/PC orientation extending from the middle of the ventricles in the superior direction: TR: 2 s, TE: 15 ms, FOV: 226×226×55 mm, spatial matrix: 32×32×8 with elliptical sampling in the sagittal (y-z) plane , nominal voxel size: 0.34 cm^3, scan time: 4:43 min. Manual placement of the MRSI slab and 8 OVS slices was performed by an experienced operator (SP). Water suppressed (WS) data were acquired with a single average using first- and second-order autoshimming and automated adjustment of water suppression. A non-water suppressed (NWS) reference scan with 1 signal average using a shorter TR (1 s) was also collected.

3D PEPSI data for automated placement of 16 OVS slices was collected from a 52 mm thick slab in AC/PC orientation extending from the basal ganglia in superior direction: TR: 2s, TE: 20 ms, FOV: 226×226×60 mm, spatial matrix: 32×32×8, elliptical sampling in the sagittal (y-z) plane, nominal voxel size: 0.37 cm^3, scan time: 4:43 min. In one subject a spatial matrix of 32×32×16 with FOV 226×226×120 mm and 10:58 min scan time was used. NWS reference scans were collected with single average using TR: 1 s.

MRSI data reconstruction and quantification

Reconstruction of PEPSI data was performed online using an ICE program that performs ramp sampling correction, removal of oversampling and separate processing of odd and even echo data. A Hamming filter was applied across all spatial dimensions to reduce peripheral lipid contamination. This filter effectively increased the voxel volume by approximately 50%. Automatic zero-order phase correction based on the (residual) water signal was applied on a voxel-by-voxel basis. Odd and even spectra were summed to obtain NWS and WS spectral arrays,. Reconstructed spectral quality was examined on the scanner in the Spectroscopy Task Card. Spectral postprocessing with LCModel fitting to generate metabolic maps was performed as described in [12].

Quantification of volume coverage in peripheral lipid containing regions and in lateral gray matter regions

The MPRAGE scans of 11 subjects were segmented using FreeSurfer (FS) segmentation pipeline (version 3.0.4) with default parameters and the resultant WM/GM surfaces were edited by an expert and used as ground truth after converting to volumetric data. Regions outside of the outer GM surface were considered peripheral lipid containing regions and CSF. The percentage coverage of peripheral lipid containing regions and CSF was computed as the fraction of MRI voxels in this region that intersects with any of the OVS slices. Due to the finite transition bandwidth and the planar geometry of the OVS slices there is unavoidable suppression of lateral gray matter (GM) and white matter (WM) regions when using a finite number of OVS slices. The percentage brain tissue (GM + WM) loss was defined as the fraction of MRI voxels in the combined GM and WM masks, within the MRSI slab, that intersects with any of the OVS slices.

Quantification of residual peripheral lipid signals

A peripheral mask was calculated based on the NWS and the WS images. Both NWS and WS were integrated along the spectral domain in magnitude mode and thresholded at 10 % signal intensity to create masks that defined the inner volume of interest and the entire imaged slab. Subtracting these two masks created the peripheral mask. For five central slices within the selected MRSI slab the residual integrated lipid signal for all voxels in the peripheral mask was computed by integrating the area under the main lipid peak (1.3 ppm) in the water suppressed data in magnitude mode over the range 1.02 ppm - 1.67 ppm,

Results

Parameter settings for image registration

The factor that affected the reliability of registration between atlas space and subject space most was the image intensity inhomogeneity. Therefore, we corrected the intensity inhomogeneities using the N3 method [28] with a relatively small smoothing distance of 50-

100 mm [29, 30]. Based on the intensity-corrected image, the correlation ratio as a similarity measure for multimodal image registration [31] was the best cost function for our data, and it resulted in the smallest position variability of the slice prescriptions (center and normal vector).

Offline validation of automatic placement of up to 16 OVS slices

When transforming the MRSI slab from MNI space (Fig. 1a) to subject space (Fig. 1c), the MRSI slab was oriented and placed at an equivalent location extending from the middle of the ventricles in superior direction, consistent with our targeted VOI for 3D MRSI. The positioning of the OVS slices in subject space (Fig. 1d) was also consistent with the placement in MNI space (Fig. 1b), forming a convex hull around the upper cerebrum. In both atlas and subject space the peripheral lipid containing regions were 100 % covered by the automatically placed OVS slices in all 11 subjects, both for 8 and for 16 OVS slices (Fig. 2).

The brain tissue loss in the 40 mm MRSI slab using 8 OVS slices was 13.9% on average for the 11 subjects (Table 1). For the 80 mm MRSI slab using 16 OVS slices the brain tissue loss was 19.3%. This difference is in part due to the use of 6 OVS slices in the superior ring for the 16 OVS slice case, which leads to a coarser coverage of peripheral regions. Furthermore, the thicker slab for the 16 OVS slice case covered more brain tissue close to the top of the head, which exhibits much stronger curvature than the brain region imaged for the 8 OVS slice case. This makes suppression more difficult and necessitates sacrificing more brain tissue closer to the top of the brain. An example of the OVS placement and the degree of suppression of lateral gray matter for the 8 OVS slice case is shown in Fig.3.

Online validation comparing automatic and manual placement of 8 OVS slices

Automated prescription of the MRSI slab and the OVS slices (steps 2 – 6 in the Method Implementation) on the external workstation took less than four minutes and was performed while a T_2 weighted scan for manual placement was acquired. As with the offline

simulations, complete coverage of peripheral lipid containing regions with automated OVS slice placement was obtained in all subjects and verified on the scanner console prior to collecting MRSI data. Volume coverage, spectral line width and lipid contamination for manual and automated OVS placement were comparable, enabling computation of metabolite maps of Ino, Cr+PCr, Glu+Gln, NAA+NAAG, and macromolecular resonances at 0.9 and 2.0 ppm. The CRLB thresholds were 20 % for NAA+NAAG, Cr+PCr, 30 % for Ins and Cho+PCho, and 50 % for Glu+Gln and MM09 (macromolecules at 0.9 ppm). Metabolite ratio maps obtained with automated OVS placement show relatively uniform metabolite distributions with distinct GM/WM contrast in Cho, Cr and Glu+Gln maps, consistent with our previous studies (Fig. 4). The slice averaged metabolite concentration ratios for the 4 central slices that are fully encompassed within the MRSI slab shown in Table 2 are comparable for automated and manual placement. They are also comparable across slices, as expected, and consistent with our previous results [12]. The number of usable voxels with CRLB threshold greater than 20 % in these maps (Table 3) was comparable across slices and metabolites, but 16 % (on average) smaller for automatic compared to manual placement, due to the more conservative choice of the OVS slice thickness for automated placement. Residual lipid signals in peripheral regions of the MRSI with automatically placed OVS slices were also comparable to data obtained with manually placed OVS slices (Table 4) and within the variability of lipid suppression ratios measured across subjects.

Online validation using automated placement of 16 OVS slices

Complete coverage of lipid containing regions was obtained in all three subjects and verified on the scanner console prior to collecting MRSI data by assessing the placement of the OVS slices (Fig. 5). The spectral quality and degree of lipid suppression was comparable to the 8 OVS slice case (Fig. 5f). Metabolite maps shown in Fig.6a display image quality comparable to our previous studies with respect to uniformity, but much larger volume coverage than previous short TE studies. The small voxel size and the stronger slab angulation in this study limited magnetic field inhomogeneity related line broadening and baseline distortion. Selected spectra from lateral and central regions in different slice

locations demonstrate comparably low levels of lipid contamination (Fig. 6b,c), confirmed by their respective LC model fits.

Discussion

This study introduces a novel method for positioning OVS slices and the MRSI slab based on an anatomical brain atlas, which eliminates the need for any operator interaction for collecting MRSI data. To our knowledge, this is the first use of atlas based registration for OVS in MRSI. This approach follows the use of statistical brain atlases in clinical settings for automatic positioning of MR imaging slices, which has become available as a product on clinical MRSI scanners. Landmark based methods have also gained popularity for positioning MRI slices in clinical imaging, but large number of landmarks would be required for placement of OVS slices due to the complex geometry of the surface of the brain, facial regions and peripheral lipid containing regions. Our data show that automatic placement of 8 OVS slices provides consistent short TE MRSI volume selection and comparable spectral quality across subjects with a similar degree of lipid suppression and number of usable voxels as manual placement. We have also demonstrated short TE MRSI with 16 automatically placed OVS slices and MRSI slab, and achieved larger volume coverage while maintaining similar spectral quality and degree of lipid suppression. The number of OVS slices is limited by T_1 relaxation during the application of the OVS modules and by nonuniformity of the B_1 field. Repetitions of the OVS modules may be required to achieve adequate suppression. Additional OVS modules to augment lipid suppression in presaturated OVS slices or to define additional OVS slices may be inserted into a spin echo sequence as shown by Chu et al [9] and during the TM period of a stimulated echo pulse sequence [6, 7].

The use of an atlas-based approach has two advantages compared to iterative optimization methods. First, the computational burden is considerably reduced facilitating integration of OVS placement into the scanner workflow. Second, iterative optimization methods may converge in local minima, resulting in suboptimal saturation band placement

and possible inter-subject variation in saturation band placement. The atlas based approach is expected to increase consistency of OVS placement and MRSI slab selection between subjects and during scan repetitions, which is advantageous for longitudinal and cross-sectional studies. Iterative optimization on the other hand is suitable for offline generation of optimal OVS slice and MRSI slab positions in atlas space under the supervision of an experienced user, who ensures that the global optimum is selected. The automated OVS positioning method by Ryner et al. [10] and Venugopal et al. [11] is based on optimization in subject space, but has not yet been applied to delineate an entire organ. The automated prescription method by Ozhinsky and Nelson, which employs prelocalization using an oblique PRESS box and 9 OVS slices to extend brain coverage, also operates in subject space [15] and is similar to our recently developed iterative optimization method [16]. These methods are capable of accurate placement of OVS slices on a subject by subject basis, but they are subject to brain segmentation errors and optimization reliability. Since they do not guarantee consistent OVS coverage and ROI positioning, these methods are not suitable for investigating spectral changes in lateral cortical regions in longitudinal studies in individual subjects and in cross-sectional studies.

The sensitive volume in this study was limited by shimming considerations rather than by the number of OVS slices. Larger volume coverage at short TE would be possible, if shimming conditions in frontal and inferior temporal cortex were improved. Reducing voxel size to 0.37 cc in this study helped mitigate magnetic field inhomogeneity in frontal brain areas and reduced spatial contamination from peripheral lipid signals.

Consistent with previous implementations of OVS slices, a planar geometry is used for OVS slices. Although this approach provides satisfactory coverage as shown in our data, there may be cases where unusual skull shapes and large thickness of peripheral regions may lead to inadequate coverage of lipid containing regions. As a potential solution, nonlinear registration using spatial normalization could be used for more accurate transformation between the atlas space and the subject space. In the future, a non-planar geometry of OVS

slice prescription from nonlinear transformation may be feasible using curved slice excitation [32], taking advantage of parallel transmit technology.

While the results of automated placement are generally comparable to those obtained with manual placement by an experienced operator, the usable volume of interest was slightly smaller than with manual placement due to conservative choice of OVS slice thickness in atlas space to accommodate inter-individual differences in local brain shapes and thickness of peripheral lipid containing regions. Subjects vary in skull and peripheral tissue thickness; thus, an optimal affine transformation for the brain may not be optimal for the skull. Hence, in the current *in vivo* experiments, we used a fixed and conservative thickness (25 mm) of the OVS slices in MNI space, which proved adequate for all subjects in our study. Further work is required to test the reliability of MRSI slab and OVS slice positioning in future test-retest studies across multiple scanners and a larger number of subjects. Further optimization of OVS slice thickness and placement in MNI space to minimize tissue loss is under evaluation. On the other hand, brain segmentation could be used online to positively identify peripheral regions to constrain the affine transformation, thus enabling thinner OVS slices to be positioned in subject space resulting in larger volume coverage.

Conclusions

We have demonstrated the feasibility of automatic and optimal placement of OVS slices based on an atlas brain. The overall quality of metabolite maps obtained when OVS slices are automatically positioned matches that of maps with manually placed OVS slices. Atlas-based prescription of the MRSI slab ensures operator independent and pre-specified selection of volume of interest across subjects. It also provides the flexibility to rapidly place large numbers of OVS slices. Moreover, it has the potential to improve the reliability of clinical 3D MRSI at short TE to reduce operator bias and improve MRSI data quality while speeding up clinical throughput. Atlas-based auto-placement prescription of MRSI slab and OVS slices is thus advantageous for longitudinal and cross sectional clinical MRSI studies

and may be integrated with automated MRI slice prescription software on clinical MR scanners.

Acknowledgement

We thank our collaborators for the opportunity to test our technology on their scanner: Dr. Steve Dager at University of Washington, Dr. John van Meter at the Georgetown University, Dr. Larry Wald at Massachusetts General Hospital and Dr. Keith Heberlein at Siemens Medical Solutions, Inc. We also thank Dr. Juan Bustillo, Akio E. Yoshimoto, MS and Elena Ackley, MS for their support and technical assistance. Part of the image processing was performed on the High Performance Cluster at The University of New Mexico Center for Advanced Research Computing (www.hpc.unm.edu). This work was supported in part by the MIND Research Network (DOE Grant No. DE-FG02-99ER62764) and the University of New Mexico School of Medicine Brain and Behavioral Illness Signature Program.

References

1. Singh S, Rutt B, Henkelman R. Projection presaturation: A fast and accurate technique for multidimensional spatial localization. J Magn Reson 1990; 87(3):567-583.
2. Singh S, Rutt BK, Napel S. Projection presaturation. II. Single-shot localization of multiple regions of interest. J Magn Reson 1990; 90(2):313–329.
3. Posse, S, Schuknecht, B, Smith, B, van Zijl, PCM, Herschkowitz, N, Moonen, CTW. Short-echo-time proton MR spectroscopic imaging. Journal of Computer Assisted Tomography, 1993; 17(1):1-14, 1993
4. Duyn JH, Gillen J, Sobering G, van Zijl PC, Moonen CT. Multisection proton MR spectroscopic imaging of the brain. Radiology 1993; 188(1):277-82.
5. Singh S, Brody WR. Projection presaturation. III. Accurate selective excitation or presaturation of the regions of tailored shape in the presence of short-T1 species. J Magn Reson B 1993; 101(1):52–62.
6. Posse, S, DeCarli, CS, Le Bihan, D. Three-dimensional Echo-Planar MR Spectroscopic imaging at short echo times in human brain. Radiology 1994; 192:733-738.
7. Posse, S, Tedeschi, Risinger, G, Ogg, R, Le Bihan, D. High Speed 1H spectroscopic imaging in Human Brain by Echo Planar Spatial-Spectral Encoding. Magnetic Resonance in Medicine, 1995; 33:34-40.
8. Tran T-KC, Vigneron DB, Sailasuta N, Tropp J, Le Roux P, Kurhanewicz J, Nelson S, Hurd R. Very selective suppression pulses for clinical MRSI studies of brain and prostate cancer. Magn Reson Med 2000; 43(1):23–33.
9. Chu A, Alger JR, Moore GJ, Posse S. Proton echo-planar spectroscopic imaging with highly effective outer volume suppression using combined presaturation and spatially selective echo dephasing. Magn Reson Med. 2003 May; 49(5):817-21.
10. Ryner L, Westmacott, G, Davison, N, Latta, P. Automated Positioning of Multiple Spatial Saturation Planes for Non-Cuboidal Voxel Prescription in MR Spectroscopy. Proceedings of the ISMRM; 2005. p 350.
11. Venugopal N, McCurdy B, Ryner L. Optimization of Outer Volume Suppression for

Improved Prostate MR Spectroscopic Imaging. Medical Physics 2006; 33(6):2183.

12. Posse S, Otazo R, Caprihan A, Bustillo J, Chen H, Henry PG, Marjanska M, Gasparovic C, Zuo C, Magnotta V, Mueller B, Mullins P, Renshaw P, Ugurbil K, Lim KO, Alger JR. Proton echo-planar spectroscopic imaging of J-coupled resonances in human brain at 3 and 4 Tesla. Magn Reson Med 2007; 58(2):236-244.
13. Henning A, Schar M, Schulte RF, Wilm B, Pruessmann KP, Boesiger P. SELOVS: Brain MRSI localization based on highly selective T1- and B1-insensitive outer-volume suppression at 3T. Mag Reson Med 2008; 59(1):40-51.
14. Henning A, Fuchs A, Murdoch JB, Boesiger P. Slice-selective FID acquisition localized by outer volume suppression (FIDOVS) for 1H-MRSI of the human brain at 7T with minimal signal loss. NMR Biomed. 2009 Aug; 22(7):683-96..
15. Ozhinsky E and Nelson SJ. Automatic prescription of 3D MRSI with optimal coverage and outer volume suppression. Proceedings of the ISMRM; 2009, p. 17.
16. Martínez-Ramón M, Gallardo-Antolín A, Cid-Sueiro J, Heileman GL. Yung KT, W. Zheng, Zhao C, Posse S. Automatic placement of outer volume suppression slices in MR spectroscopic imaging of the human brain. Magnetic Resonance in Medicine, 2010; 63(3):592-600.
17. Van der Kouwe AJ, Benner T, Fischl B, Schmitt F, Salat DH, Harder M, Sorensen AG, Dale AM. On-line automatic slice positioning for brain MR imaging. NeuroImage 2005; 27(1):222–230.
18. Benner T, Wisco JJ, van der Kouwe AJ, Fischl B, Vangel MG, Hochberg FH, Sorensen AG. Comparison of manual and automatic section positioning of brain MR images. Radiology 2006; 239(1): 246-54.
19. Evans AC CD, Mills SR, Brown ED, Kelly RL, and Peters TM. 3D statistical neuroanatomical models from 305 MRI volumes. IEEE-Nuclear Sci Symp Med Imagine Conf 1993. p 1813-1817.
20. Smith SM, Jenkinson M, Woolrich MW, Beckmann CF, Behrens TE, Johansen-Berg H, Bannister PR, De Luca M, Drobnjak I, Flitney DE, Niazy RK, Saunders J, Vickers J, Zhang Y, De Stefano N, Brady JM, Matthews PM. Advances in functional and structural MR image analysis and implementation as FSL. Neuroimage 2004; 23 Suppl 1:S208-219.

21. Provencher SW. Estimation of metabolite concentrations from localized in vivo proton NMR spectra. Magn Reson Med 1993; 30(6):672-679.
22. Smith SM. Fast robust automated brain extraction. Human Brain Mapping. 2002; 17(3): 143-155.
23. Ashburner J, Friston KJ. Rigid body registration. In R.S.J. Frackowiak, K.J. Friston, C. Frith, R. Dolan, K.J. Friston, C.J. Price, S. Zeki, J. Ashburner, and W.D. Penny, editors, Human Brain Function. Academic Press, 2nd edition, 2003.
24. M. Jenkinson, P.R. Bannister, J.M. Brady, and S.M. Smith. Improved optimisation for the robust and accurate linear registration and motion correction of brain images. NeuroImage, 2002; 17(2): 825–841.
25. Ashburner J, Friston KJ. Rigid body registration. In R.S.J. Frackowiak, K.J. Friston, C. Frith, R. Dolan, K.J. Friston, C.J. Price, S. Zeki, J. Ashburner, and W.D. Penny, editors, Human Brain Function. Academic Press, 2nd edition, 2003.
26. Jenkinson M, Bannister PR, Brady JM, Smith SM. Improved optimisation for the robust and accurate linear registration and motion correction of brain images. NeuroImage, 2002; 17(2):825–841.
27. Sabuncu M, Yeo BTT, Vercauteren T, Van Leemput K, Golland P. Asymmetric Image-Template Registration. Proceedings of the 12th International Conference on Medical Image Computing and Computer Assisted Intervention (MICCAI 2009), September 20 - 24 2009, London, UK.
28. Sled JG, Zijdenbos AP, Evans AC. A nonparametric method for automatic correction of intensity nonuniformity in MRI data. IEEE Transactions on Medical Imaging 1998; 17(1):87-97.
29. Boyes RG, Gunter JL, Frost C, Janke AL, Yeatman T, Hill DLG, Bernstein MA, Thompson PM, Weiner MW, Schuff N, Alexander GE, Killiany RJ, DeCarli C, Jack CR, Fox NC. Intensity non-uniformity correction using N3 on 3-T scanners with multichannel phased array coils. NeuroImage 2008; 39(4):1752-1762.
30. Zheng W, Chee M WL, Zagorodnov V. Improvement of brain segmentation accuracy by optimizing non-uniformity correction using N3. NeuroImage 2009; 48(1):73-83.
31. Roche A, Malandain X, Pennec X, Ayache N. The correlation ratio as a new similarity

measure for multimodal image registration. In Proc. Of First Int. Conf. on Medical Image Computing and Computer-Assisted Intervention (MICCAI'98), Vol. 1496 of LNCS, p. 1115-1124, Cambridge, USA, October 1998. Springer Verlag.

32. Boernert P, Schaffter T. Curved slice imaging. Magn. Reson. Med. 1996; 36(6):936-939.

Subject	Brain tissue loss for 16 OVS slices [%]	Brain tissue loss for 8 OVS slices [%]	Increase in brain volume coverage - 16 vs. 8 OVS slices
1	9.79	10.74	1.6069
2	22.07	12.79	1.5979
3	22.71	13.42	1.6032
4	16.22	9.68	1.5816
5	22.39	14.67	1.5651
6	22.75	13.60	1.5882
7	16.67	9.46	1.6105
8	18.04	11.27	1.5958
9	19.12	17.88	1.6085
10	23.32	21.31	1.5772
11	18.78	17.89	1.5767
Mean (SD)	**19.26 (4.07)**	**13.88 (3.79)**	**1.59 (0.02)**

Table 1: Offline computation of brain tissue loss in lateral gray matter due to automated placement of 16 versus 8 OVS slices and increase in brain volume coverage for 16 versus 8 OVS slices using MPRAGE data collected in 11 subjects. Brain tissue loss is computed with respect to the brain volume encompassed by the MRSI slab.

Slice	Placement Method	Glu+Gln/Cr +PCr	NAA+ NAAG/Cr+ PCr	tCho/Cr+PCr	Ins/Cr+PCr	MM09/Cr+ PCr
3	Automatic	1.08(0.53)	1.17(0.43)	0.26(0.11)	1.08(0.33)	1.43(0.65)
	Manual	1.56(0.52)	1.37(0.73)	0.44(0.12)	1.02(0.33)	1.24(0.45)
4	Automatic	1.26(0.68)	1.29(0.43)	0.26(0.10)	1.05(0.31)	1.64(0.70)
	Manual	1.21(0.57)	1.25(0.44)	0.24(0.09)	1.03(0.29)	1.47(0.53)
5	Automatic	1.32(0.37)	1.14(0.37)	0.22(0.08)	0.92(0.33)	1.37(0.56)
	Manual	1.43(0.64)	1.24(0.36)	0.24(0.08)	0.96(0.27)	1.44(0.51)
6	Automatic	1.68(0.66)	1.45(0.57)	0.23(0.10)	0.90(0.33)	2.20(0.92)
	Manual	1.15(0.38)	1.26(0.35)	0.26(0.08)	0.97(0.28)	1.45(0.38)
Mean (SD)	**Automatic**	**1.34 (0.25)**	**1.26 (0.14)**	**0.25 (0.02)**	**0.99 (0.09)**	**1.66 (0.38)**
Mean (SD)	**Manual**	**1.34 (0.19)**	**1.28 (0.06)**	**0.29 (0.10)**	**1.00 (0.03)**	**1.40 (0.11)**

Table 2: Slice averaged metabolite concentration ratios with respect to Cr+PCr (standard deviation) in metabolite maps measured with automatic and manual placement of 8 OVS slices as a function of slice position within the MRSI slab.

Slice	Placement Method	Glu + Gln	NAA+ NAAG	Cr + PCr	tCho	Ins	MM09
3	Automatic	212	237	235	213	229	234
	Manual	265	266	284	248	271	292
4	Automatic	225	223	226	207	223	277
	Manual	252	259	249	227	248	252
5	Automatic	206	206	211	181	197	231
	Manual	232	229	225	203	218	257
6	Automatic	205	189	195	162	188	242
	Manual	284	269	281	259	284	242
Mean (SD)	**Automatic**	**212.0 (9.2)**	**213.7 (20.8)**	**216.8 (17.6)**	**190.8 (23.7)**	**209.3 (19.8)**	**246.0 (21.2)**
Mean (SD)	**Manual**	**258.3 (21.9)**	**255.8 (18.3)**	**259.8 (28.1)**	**234.3 (24.7)**	**255.3 (29.0)**	**260.8 (21.7)**

Table 3: Number of voxels above threshold in metabolite maps acquired with automatic and manual placement of 8 OVS slices as a function of slice position within the MRSI slab for 3D data set with 8 encoded slices.

Slice	Automatic Placement	Manual Placement
3	1.00	0.86
4	1.00	0.91
5	0.97	0.94
6	0.86	0.89
7	0.85	0.63
Mean (SD)	**0.94 (0.07)**	**0.84 (0.13)**

Table 4: Comparison of the integrated residual lipid signal for automatic and manual placements for five slices of selected 3D PEPSI data sets with 8 encoded slices. The integrated lipid signal (arbitrary units) is scaled to the maximum in slices 3 and 4 of the data set acquired with automated placement.

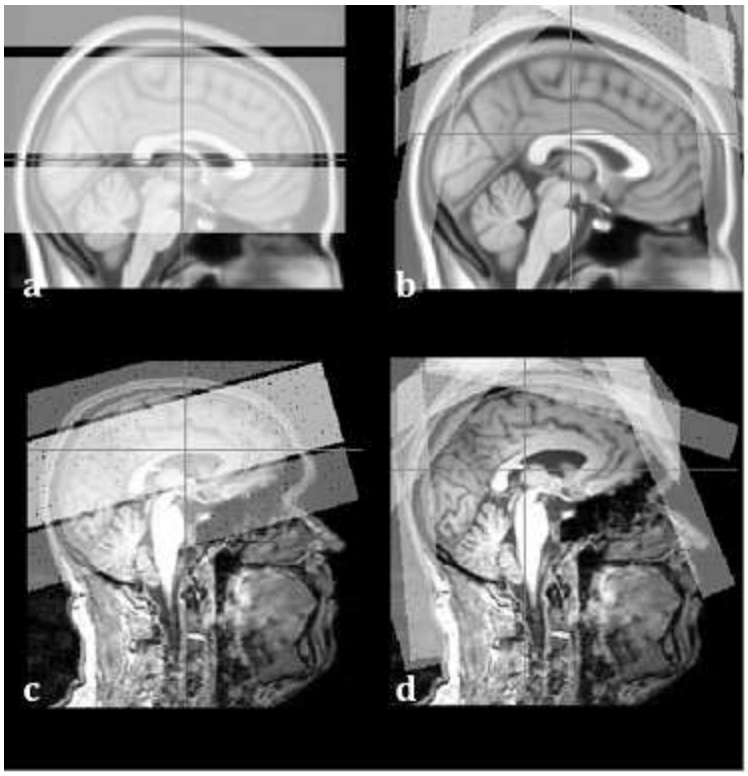

Figure 1: Placement of MRSI slab and 16 OVS slices on the MNI template head and transformation to the subject head, displayed in the mid-sagittal plane, in offline computation. The MRSI slab and OVS slices 1 and 16 are depicted in the MNI head (a) and mapped onto the subject's head (c). OVS slices 2 through 15 are displayed on the MNI head (b) and mapped onto the subject's head (d).
98x103mm (96 x 96 DPI)

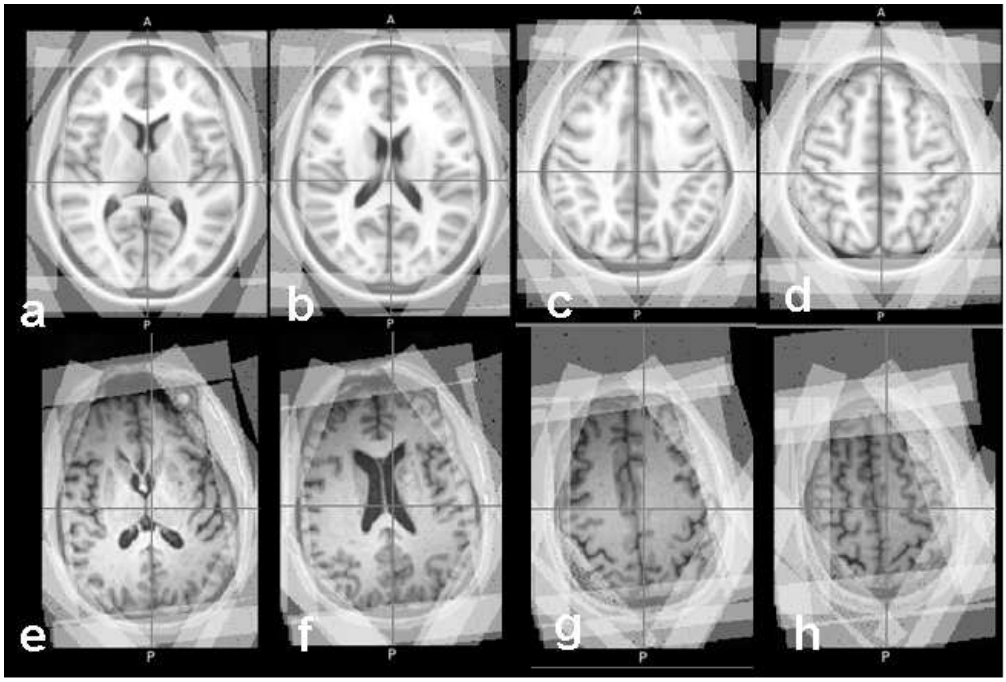

Figure 2: Offline computation of 16 automatically positioned OVS slices in MNI space (top) and their transformed positions in subject space (bottom) in four different axial slice positions along the inferior to superior direction (a, z = 80 mm; b, z = 90 mm; c, z = 110 mm; and d, z = 120 mm).
173x116mm (96 x 96 DPI)

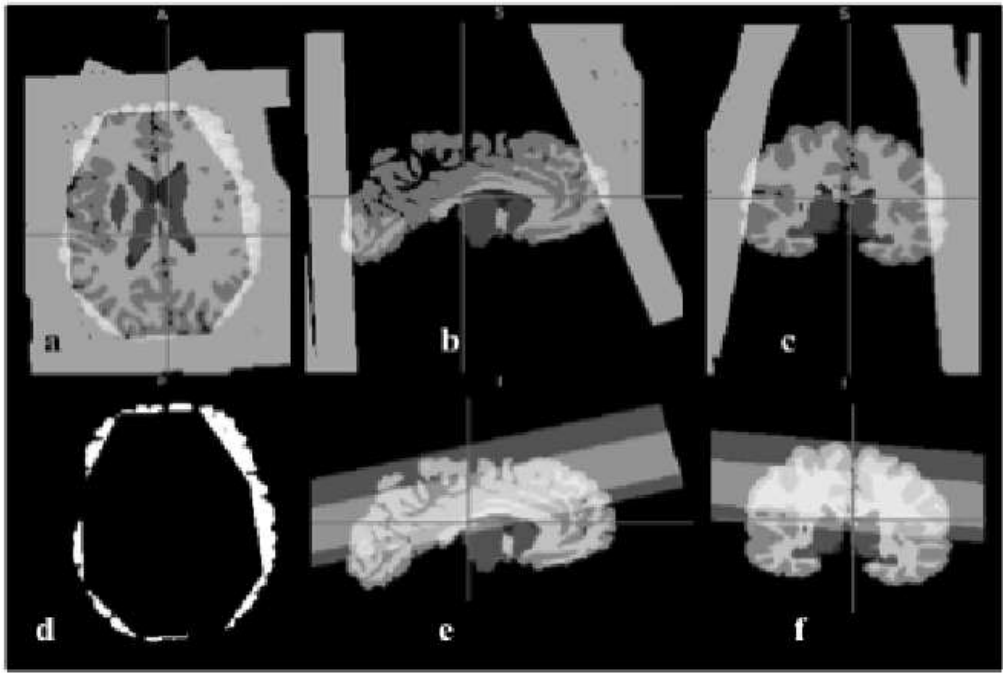

Figure 3: Offline computation of the overlap of brain tissue with the OVS slices in cortical regions in axial (a), sagittal (b), and coronal (c) orientations in an individual's brain. (d) Cortical tissue covered by 16 OVS slices in axial view at the same axial slice level as in (a) . Sagittal (e) and coronal (f) views of the intersection of the brain volume with the 80 mm MRSI slab (light + dark gray regions) and the 40 mm slab (light gray region).
173x116mm (96 x 96 DPI)

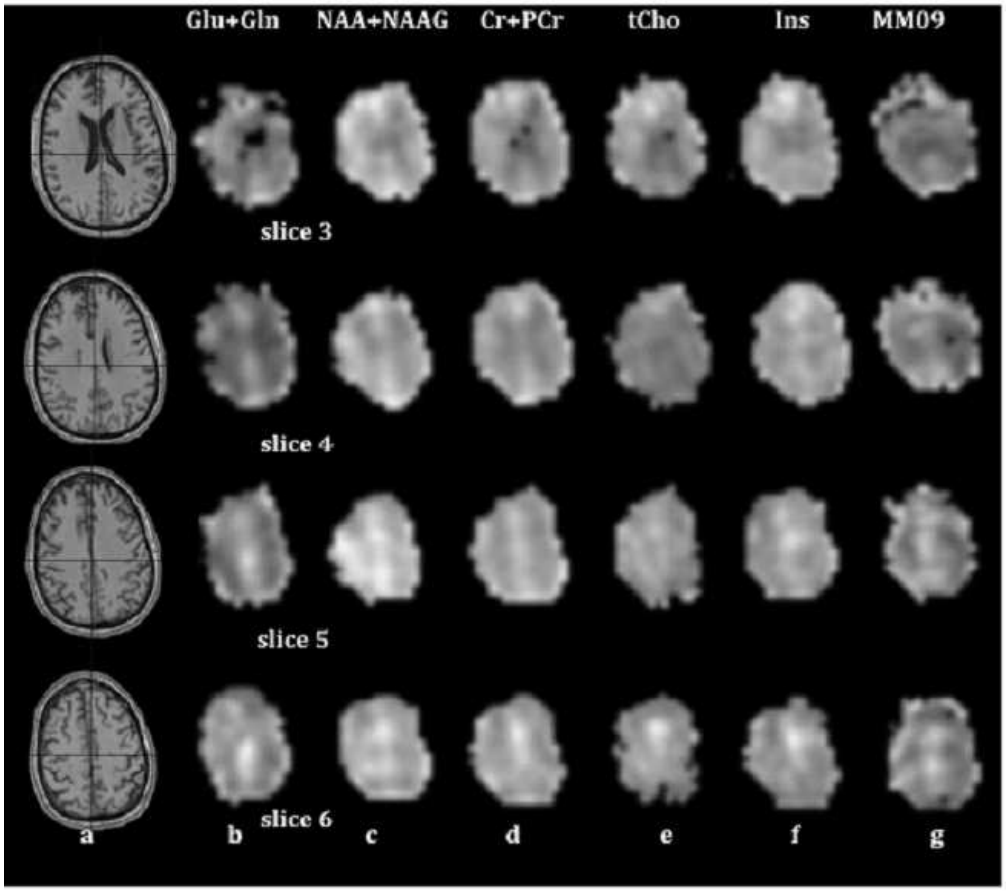

Figure 4: Metabolite maps obtained with automated placement of 8 OVS slices: (a) MRI, (b) Glu+Gln, (c) NAA+NAAG, (d) Cr+PCr, (e) tCho, (f) Ins, and (g) MM09.
172x153mm (96 x 96 DPI)

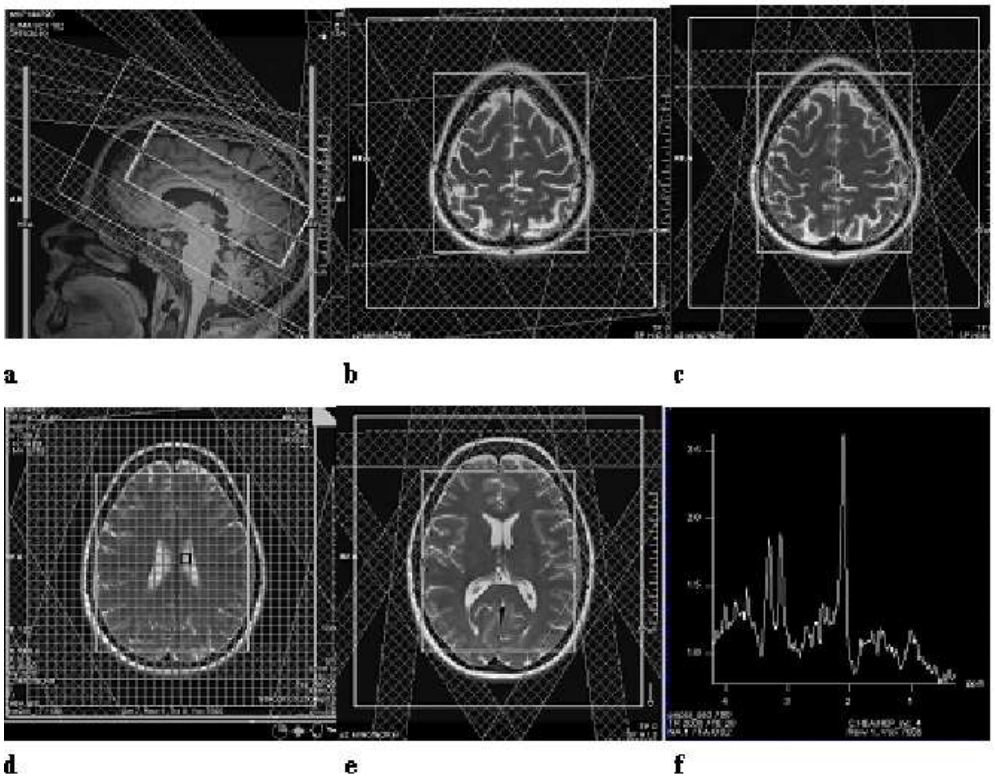

Figure 5: Automated placement of 16 OVS slices in vivo shown on the scanner console in (a) sagittal orientation and at (b, c, d, e) different axial slice levels. The superior slice locations in (b) and (c) depict the upper ring with 6 OVS slices. The inner box is the shim region. The outer box delineates the field of view. The spectral grid in (d) shows the size of the encoded voxels and the localization of the 6 OVS slices from the upper OVS ring, which are outside of the head at this axial location. The inferior slice location in (e) depicts 7 of the 8 OVS slices that are part of the lower OVS ring. A representative spectrum from the scanner console with 0.38 cc acquired in 10:58 min is shown in (e). The only spectral processing that was applied was mild exponential filtering.
177x141mm (96 x 96 DPI)

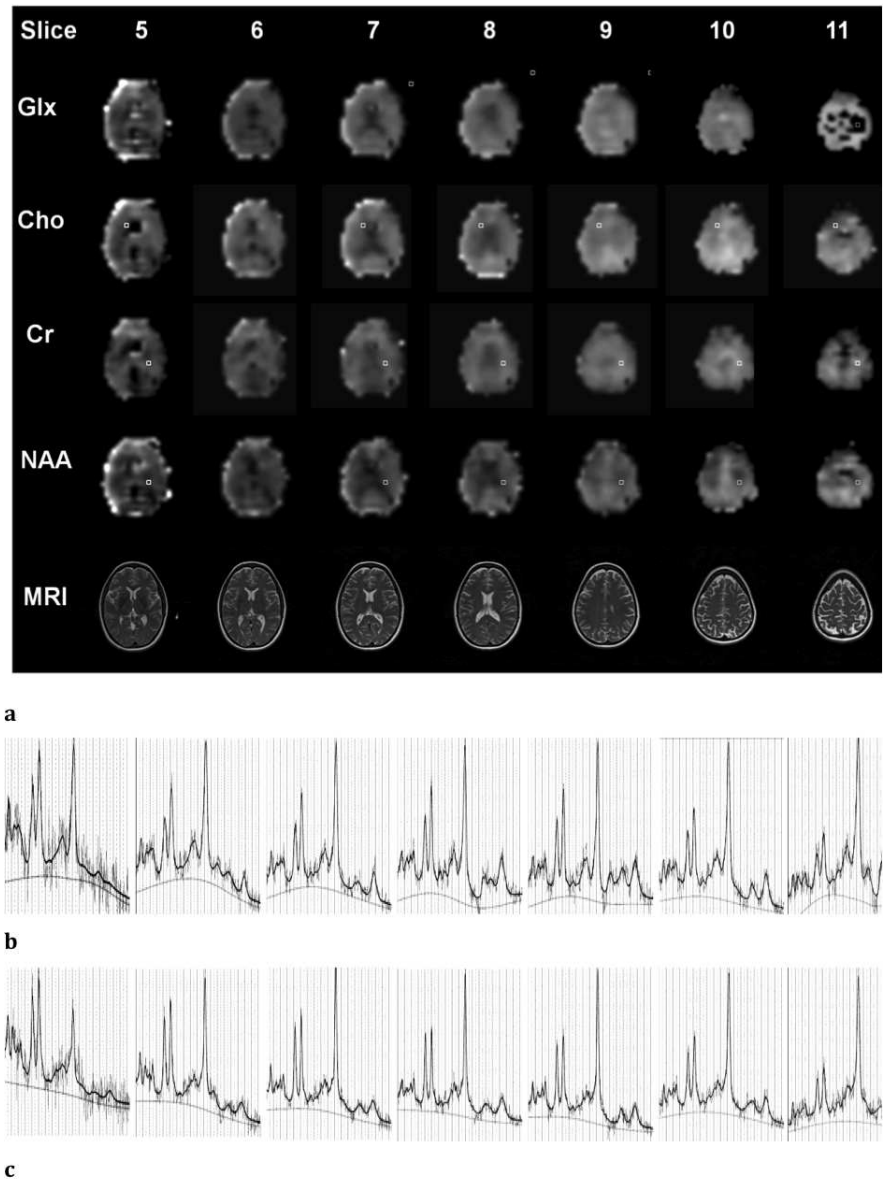

Figure 6: a) Metabolite maps of Glu+Gln, Cho, Cr and NAA obtained with automated placement of 16 OVS slices and 32x32x16 spatial matrix. The 7 slices represent the 52 mm thick slab selection. b) Selected representative spectrum from a left lateral voxel at a distance of 7 mm from the OVS slice for each of the 7 slices. c) Selected representative spectra from central brain regions for each of the 7 slices. The displayed spectral range is 0.2-4.2 ppm.
159x217mm (150 x 150 DPI)